Computational Modeling of Hole Distortion in Extruded Microstructured Optical Fiber Glass Preforms

Mohamed Trabelssi, Heike Ebendorff-Heidepriem, Kathleen A. Richardson,
Tanya M. Monro, and Paul F. Joseph

***Abstract*—Extrusion of glass preforms that are used to draw microstructured optical fibers was simulated using computational mechanics. The study focused on a preform with a cross-section geometry that contains 36 holes arranged in three hexagonal rings. Symmetry allowed for the modeling of a thirty degree portion of the cross-section, which included five holes within this reduced computational domain. The simulations took into account flow through an array of 13 feed holes, flow along five circular pins to create the holes, exit from the die and the development of a constant profile for the cross section of the preform. The primary concern in the study was exploring the capacity of the model to reproduce the observed distortion of the extruded holes, i.e., the difference between the holes that develop and the negative of the pin arrangement, by taking into account the complexity of the flow. The key features that describe the model are viscous flow, uniform temperature, interface slip using the Navier friction model and the assumption of a steady-state solution. Validation of the procedure was based on a comparison between the predicted cross-section and an actual preform. The results show that distortion of the holes is rather sensitive to the level of friction, which provides insight into reducing the magnitude of distortion in future experimental work.**

***Index terms*—Computational, Extrusion, FEM, Friction, Glass Preform, Microstructured Optical Fiber, Photonic Crystal Fiber, Wall Slip**

This material is based upon work supported by the U.S. Army Research Laboratory and the U. S. Army Research Office under contract/grant number ARO No. 56858-MS-DPS and through funding from the National Science Foundation, DMR #0807016. TMM acknowledges support of ARC Federation and Laureate Fellowships, ARC grant DP0880436 and ARC Centre of Excellence in Nanoscale Biophotonics (CNBP).

M. Trabelssi and P. F. Joseph are with the Department of Mechanical Engineering, Clemson University, Clemson, SC 29634-0921, USA (e-mail: mtrabel@g.clemson.edu, jpaul@clemson.edu)

H. Ebendorff-Heidepriem and T. M. Monro are with the Institute of Photonics and Advanced Sensing and ARC Centre of Excellence for Nanoscale BioPhotonics, The University of Adelaide, Adelaide, SA 5005, Australia (e-mail: heike.ebendorff@adelaide.edu.au, tanya.monro@adelaide.edu.au)

K. A. Richardson was with the Department of Materials Science and Engineering, COMSET, Clemson University, Clemson, SC and is currently at the College of Optics and Photonics, CREOL, University of Central Florida, Orlando, FL 32816, USA (e-mail: kcr@creol.ucf.edu).

I. Introduction

The billet extrusion process for the manufacture of preforms used to draw microstructured optical fibers (MOFs) has been shown to be a robust and versatile approach that works for a wide range of glass types [1,2]. Contrary to other approaches such as stacking [3,4], drilling [5-7] and casting [8,9] which have limitations in terms of geometry [10] and surface quality [11-13], billet extrusion appears to provide a nearly unlimited range of possibilities in terms of the geometric arrangement of holes that can be achieved within a cross-section [1,2]. To reach its full potential, however, for some preform shapes [1,14] it is necessary to account for distortion and drift of the holes in the preform, i.e., the difference between the pattern of the die exit and that of the final preform, in order to optimize die design to achieve a targeted geometry. The importance of a precise hole pattern for realizing specific optical characteristics has been studied in [15-17]. These computational studies, which focus on the optical characteristics of an existing fiber, show how imperfect geometries prevent the predicted optical properties of the fiber designs from being achieved, and this is especially problematic for distortions that are located closer to the core of the fiber.

In the current study, the impact of glass flow in complex dies on hole distortion and drift is demonstrated using computational modeling of the extrusion process. The distortion of the holes within a glass preform is analogous to lens profile deviation in precision lens molding [18]. Just as the final lens takes on a different shape from the mold, the final cross section of the preform has geometry different than that defined by the pins, both in shape and location. Furthermore, in the manufacture of precision lenses and MOFs a relatively high viscosity in the range of $10^7 – 10^9$ Pa·s must be used. Therefore, interface slip between the glass and die/mold surface occurs [19-23], which has been shown to affect size and shape [22,24] of the resulting component.

II. Die Geometry

In this paper, a die type that is used to extrude preforms with cladding holes arranged in a concentric hexagonal

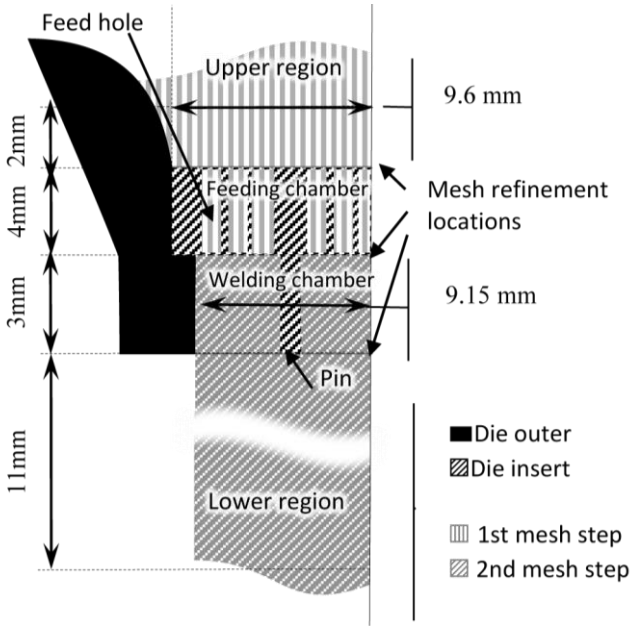

Fig 1. Die insert chambers and modeling domains used in the convergence study.

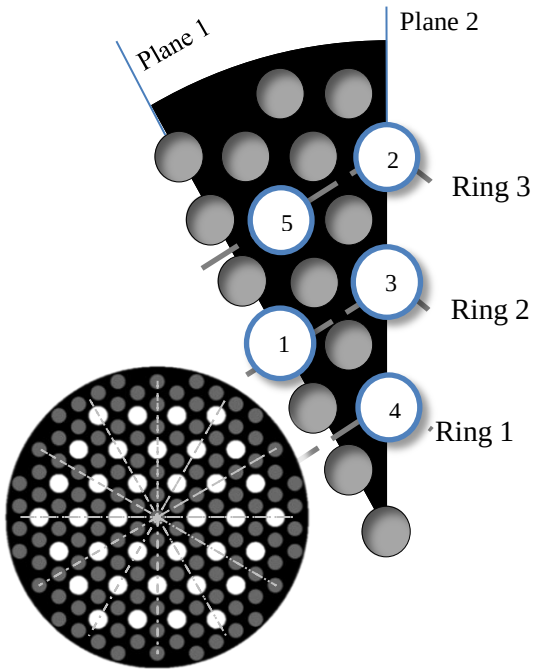

Fig 2. Feed holes (grey), pins (white) and symmetry planes in the full die insert cross-section and the thirty degree region used in the simulations.

structure is considered. The MOFs made from such preforms are referred to as photonic crystal fibers (PCFs).

The primary feature in the computational model is in accounting for the geometric complexity of the die consisting of a die outer and a die insert as shown in the schematic in Figure 1. Compared to extrusion of a solid rod [22], the die includes an insert consisting of a disk with feed holes and protruding pins [25]. Referring to Figure 1, the insert forms two chambers. The leading chamber has a pattern of axially aligned feed holes within a circular disk and is called the feeding chamber. The feed holes control the glass flow into the welding chamber, which consists of a pattern of axially aligned pins that are supported by the disk. The holes in the preform are created as glass flows over the end of the pins. This pattern creates the lattice of holes in the cross-section of the preform.

Each group of feed holes belonging to the same hexagon is called a feed hole ring. Similarly, each pin group arranged in the same hexagon is called a ring. In the present study, the pins and the feed holes have been organized in the design presented in Figure 2. The pattern duplicates what was used in the studies of Ebendorff-Heidepriem and Monro [1, 23], and was based on the limited geometrical data made available in those studies. Specifically, the feed hole diameters were given as 0.8 mm, the feeding chamber length was 4 mm and the pin diameters were 1 mm [1,23]. Referring to Figure 1, the welding chamber length (same as pin length), the welding chamber diameter and the diameter of the exit of the upper region were not provided. While the actual (confidential) values from the experiment were used for all the results presented in this paper, values as defined in Figure 1 were selected for performing the convergence study.

The geometry in Figure 2 reveals how a 30 degree portion with only five different pins is sufficient to analyze the entire cross-section when symmetry is taken into account. The reference system for the pins is also provided in this figure.

While taking advantage of symmetry provides a simplification of the complete model, the remaining structure is still fairly complicated due to the presence of 13 feed holes and 6 free surfaces.

The key point in this study is that the resulting pattern of holes in the preform caused by a particular feed hole and pin arrangement is not the precise negative of the pins. Due to the complexity of the glass flow, the cross section of the preform undergoes deformations as the glass exits the welding chamber and continues to rearrange beyond the die exit. Essentially the mechanism of "die swell" occurs throughout the cross section, which enlarges the cross section as the flow exits the die, and also changes the location and shape of each hole as the flow exits the end of each pin. While the hexagonal structure of the holes in the preform is relatively similar to its pin negative for the entire cross section of the preform, from an optical point of view the distortions in the shape and position of each hole can be significant [15-17]. An understanding of the flow mechanisms that lead to these changes in the cross section is required.

III. Numerical Experiment with Structural Relaxation

In this section the impact on hole distortion due to heating and cooling are considered to see if temperature non-uniformity should be accounted for in the modeling. Based on experience with precision lens molding, structural relaxation (temperature history dependent thermal expansion) was shown to be a dominant mechanism for the shape change of a lens [18, 24]. In order to understand the role of structural relaxation in MOF extrusion, a numerical experiment was performed in which a stress-free glass preform was cooled

from a typical extrusion temperature to room temperature, using the thermo-mechanical viscoelastic material parameters for L-BAL35 glass obtained from Ananthasayanam et al. [18]. The objective was to determine the order of magnitude of the distortion due to the complex thermal effects encountered during heating and cooling relative to the experimentally observed cross-sectional distortion from Ebendorff-Heidepriem and Monro [1]. The computational results [26] revealed that the displacement field had to be magnified by a factor of 500,000 in order to have the distortion on the same scale as that of the extruded preform. The results show that glass structural relaxation cannot account for the large shape change observed in such preforms and can be neglected.

Further simplification in the modeling can be made based on how the glass is heated. In an extrusion trial, the glass and die are first heated up to and allowed to equilibrate at the fixed extrusion temperature before the force is applied. During the extrusion process, the extrusion temperature is kept constant within less than ±1 ^{o}C. The die exit is situated within the hot zone of the furnace. Based on these experimental conditions, it was assumed that the glass within the die and for a short length below the die exit is heated sufficiently to achieve a uniform temperature and this temperature is maintained during the extrusion, i.e., cooling as the preform exits the die is neglected. Therefore, the simulations assume uniform temperature, which is reflected by constant viscosity.

IV. Computational Model

A. Governing Equations, Boundary Conditions and Model Assumptions

The Eulerian interpretation is used to simulate the extrusion process. The governing equations are given by the continuity and conservation of momentum equations as follows:

$$\frac{\partial \rho}{\partial t} + \nabla \cdot (\rho \mathbf{u}) = 0, \tag{1}$$

$$\rho\left(\frac{\partial \mathbf{u}}{\partial t} + \mathbf{u} \cdot \nabla \mathbf{u}\right) = -\nabla p + \nabla \cdot \mathbf{T} + \mathbf{f}, \tag{2}$$

where ρ is the density of the glass, $\mathbf{u}$ is the velocity vector, p is the pressure, $\mathbf{T}$ is the deviatoric stress tensor and $\mathbf{f}$ are the body forces. When inertia and gravity forces are neglected and when steady state extrusion of an incompressible Newtonian fluid is considered, where $\mathbf{T} = \eta \nabla \mathbf{u}$ and η is the shear viscosity, the equations reduce to:

$$\nabla \cdot \mathbf{u} = 0, \tag{3}$$

$$\nabla \cdot (\eta \nabla \mathbf{u}) - \nabla p = 0. \tag{4}$$

Following the die swell study by Trabelssi, et al. [22], inertia and gravity can be neglected due to the high viscosity (> 10^7 Pa·s) and low ram speed (< 0.5 mm/min for a billet diameter of about 30 mm) that are required to achieve the desired optical quality. A key assumption made in the current study is that steady state has been achieved, which neglects the transient phase as the glass flows through the feed holes and merges in the welding chamber. Indeed for some processing conditions such merging does not occur properly, which leads to a failed extrusion. The current study did not address this possibility and assumes a successful extrusion where the focus is on distortion of the holes. To make an analogy with the actual process, the steady state assumption is equivalent to assuming that the glass fills all chambers before extrusion starts. The effect of surface tension on hole distortion is also neglected due to high viscosity. While the viscosity level helps to simplify the problem in the above mentioned ways, it also makes interface slip more likely; thus it cannot be neglected. Following Trabelssi et al. [22] and Trabelssi and Joseph [20], the linear form of the Navier friction model is used to describe the interface behavior between the glass and the die. In this model the interface friction, τ_{wall}, is related to the relative sliding speed between the die and the glass, u_{wall}, by

$$\tau_{wall} = k u_{wall}, \tag{5}$$

where k is the Navier friction coefficient. As discussed by Trabelssi and Joseph [20], a non-dimensional form of the friction coefficient is given by $k \times m/\eta$, where "m" corresponds to a unit of a meter, the viscosity is given in Pa·s, shear stress is in Pa and the sliding speed is in m/s. In the current study the logarithmic form, $\log(k \times m/\eta)$, will be used for this parameter. Furthermore, the level of friction is assumed to be the same at all surfaces where glass contacts the die outer and the die insert with the feed holes and the pins. To better understand the magnitude of the normalized friction coefficient, in the die swell study by Trabelssi et al. [22] normalized friction coefficients in the range of $2.5 < \log(k \times m/\eta) < 3.5$ were obtained for three different glass types contacting a stainless steel die for the same viscosity range of interest as the current study. Furthermore, in the extrusion study by Trabelssi, et al. [22], a no-friction response occurred for approximately $\log(k \times m/\eta) < -1$ while no-slip occurred around $\log(k \times m/\eta) > 8$, which gives an active range of the normalized friction parameter as $-1 < \log(k \times m/\eta) < 8$. Trabelssi [26] demonstrated this range also applies to the current study, however in general the range depends on the physical problem. For example, for the ring geometry considered by Trabelssi and Joseph [20], the active range was approximately $-2 < \log(k \times m/\eta) < 6$.

The boundary conditions must be defined on four surfaces: inflow, outflow, free surfaces and the die/glass interfaces. The free surfaces include the holes and the outer surface of the extruded preform in the lower region. The interfaces occur at the feed holes, the pins and the outer walls of the upper region and the welding chamber. At the inflow of the upper region the radial component of velocity vanishes and the flow rate

$$Q = 2\pi \int_0^R u_z r dr, \tag{6}$$

must be specified. At the outflow of the computational domain tangential velocities are zero and the normal stress in the axial direction is zero since gravity is neglected. Upon emergence from the die all surfaces of the MOF preform are free of stress. Along all die/glass interfaces tangential velocities are imposed and the friction condition, Equation (5), applies. Finally, along Planes 1 and 2, which are defined in Figure 2, symmetry requires no flow in the circumferential direction and the shear stress components, $\tau_{\theta z}$ and $\tau_{r\theta}$, are zero.

The flow profile at the inflow was simplified by replacing the actual die shape upstream of the feed holes by a right circular cylinder with a radius slightly larger than the disk radius. Thus, at the inflow the flow rate Q was applied with a velocity profile that corresponded to an axisymmetric flow in a long cylinder with the same conditions of friction at the wall. The two extremes of plug flow and Poiseuille flow correspond to the no-friction and no-slip limits, respectively. Following Trabelssi and Joseph [20] and Trabelssi et al. [22], who demonstrated that for a given problem the final shape depended on only the ratio of k/η, it was determined that the distortion results in the current study had this same dependence. Values of viscosity used to test this behavior ranged from 10^7 to 10^9 Pa·s, which corresponds to the operational range in experimental studies of optical preform extrusion [1, 23]. Similarly, Trabelssi and Joseph [20] showed that the friction calibration curves were not a function of the flow rate for the linear form of the friction law given by Equation (5). In the current study it was determined that the distortion results were also independent of flow rate. Thus, the results presented in this study were obtained by varying k for constant values of viscosity and flow rate, which were taken as $\eta = 10^8$ Pa·s and $Q = 6.0960\times10^{-10}$ m^3/s for the full cross section. Note that such viscosity and flow rate values have been used experimentally to extrude MOF preforms.

B. The Computational Domain

Referring to Figure 1, the length dimensions that define the outer boundaries of the upper and lower regions of the computational model had to be determined. Contrary to the feeding and welding compartments that are physical parts of the die, the two regions in Figure 1 are introduced for computational reference. The dimensions of these regions were based on convergence of the final shapes and locations of the five holes, which were the convergence parameters used throughout this study. Furthermore, convergence was defined as having a result within 1% of the corresponding result for the most detailed model that could be achieved. Minimum values of the length of the computational domain above the feeding chamber (upper region) and the length of the preform (lower region) were determined to reduce computational cost yet still achieve a sufficient level of convergence. The length of the upper region, which was modeled as a cylinder, is important to allow a smooth reorganization of the flow from its axisymmetric inflow to the correct profile as it enters the feed holes. Similarly, the lower region must be long enough to allow the correct cross-sectional length-independent profile to develop. Details of this convergence study are provided in [26] and the final dimensions of the model are presented in Figure 1.

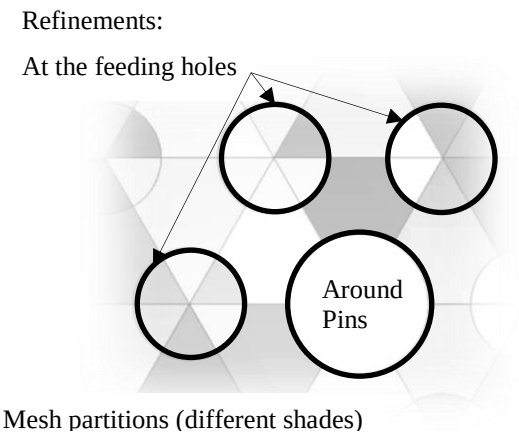

Fig. 3. Regions of mesh refinement.

The convergence study was performed for a very high value of friction which was determined to be the most difficult case to converge.

C. Mesh presentation and convergence

To achieve accuracy a refinement of the mesh was required in several locations, which are indicated in Figures 1 and 3. For a given pattern of feed holes, convergence becomes more difficult as the space between the feed holes and the pins decreases, since smaller elements are required to capture the high gradients due to boundary layer effects, especially for high values of friction. Convergence with respect to the mesh was a task coupled with the above determination of the sizes of the upper and lower regions. Furthermore, additional details of the convergence study were presented by Trabelssi [26], where two different die insert patterns were considered. The convergence results presented below correspond to the more complex of the two patterns and therefore apply to both.

The mesh was based entirely on sweeping meshed surfaces in the axial direction for each of the compartments of the die. Thus the mesh is completely free of tetrahedral elements and is dominated by brick elements (there are a few triangular prisms). Referring to Figure 1, due to the complexity of the geometry several levels of refinement are required at the glass/die boundaries, around all free surfaces, and at both ends of the die compartments. The geometric complexity requires a relatively large number of elements, which requires significant computational power. To create a reasonably uniform distribution of elements throughout each cross section, extra partitions were added along the local symmetry planes identified in Figure 3.

D. Mesh convergence study

Unlike glass extrusion of a solid rod such as in the study by Trabelssi et al. [22], as shown in Figure 1 the flow in the MOF extrusion process is divided into the upper region, the feeding chamber, the welding chamber and the lower region. Given the identification of the lengths of the upper and lower regions as discussed in the previous section, the flow can be

divided into two major stages. The first stage is composed of the upper region and the feeding chamber. The primary focus of this stage is to distribute the glass flow among the feed holes and have the flow emerge into the welding chamber using a free outflow boundary condition. The second stage consists of flow through and beyond the welding chamber, which forms the final preform. The flow in the second stage depends on convergence of the flow in the first stage. Therefore, mesh convergence was achieved in two steps. In the first step only the mesh density within the upper region and the feeding chamber was studied. Based on this convergence study, the subsequent step studied the mesh density of the remaining region to ensure the convergence of the final shapes of the five holes within the preform.

In the first stage, models of about 37,000, 76,000 and 130,000 elements were used. In the second stage configurations of about 84,000, 108,000, 148,000, 202,000 and 224,000 elements were used. Through a systematic procedure including the coupling of the two stages, it was determined that the lowest density model for the first stage combined with the case of 108,000 elements for the second stage provided convergent results as compared to results from the two highest element meshes.

V. Results

The primary focus of the study is the drift and the distortion of the holes, i.e., the difference between the location, size and shape of the pins and their resulting holes created in the MOF preform following extrusion. The distorted hole shapes as a function of the normalized Navier friction parameter for the five holes as defined in Figure 2 are presented in Figure 4. The results show the strong dependence of distortion of the holes on friction and pin location. It is also noted that even for no friction, which corresponds to the case of $\log(k \times m/\eta) = -2$, the holes experience drift and shape change due primarily to in-plane flow and non-uniform axial flow at the die exit for this welding chamber length. For example, at the die exit the magnitude of the in-plane flow for the no friction case is about 1/20 that of the no-slip case as defined by either maximum or average values. As shown by Trabelssi [26], flow rate through the feed holes is nearly uniform for all levels of friction so the no friction case requires less rearrangment as it flows through the welding chamber. To visualize how the distortion in Figure 4 affects the actual preform, in Figure 5 a quarter of the entire cross section of the preform is presented for four different friction coefficients.

Given the capability demonstrated by the results in Figure 5, a visual validation with the experimental results from Ebendorff-Heidepriem and Monro [1] can be made by selecting a friction coefficient that leads to a best match of the hole shapes and the die swell. Comparisons between the experimental and computational results are presented in Figure 6 for such a friction coefficient ($\log(k \times m/\eta) = 4.29$). Given the severe distortions that can occur, the comparison in this figure demonstrates the accuracy of the model.

In order to better understand how friction affects the distortion, axial and in-plane flow profiles at a section halfway through the welding chamber are provided in Figure 7. This figure takes advantage of the 30 degree symmetry to provide solutions for three different levels of friction in one plot. The results show the complexity of flow in the welding chamber and how in-plane flow and non-uniform axial flow, which contribute to distortion, increase as friction increases.

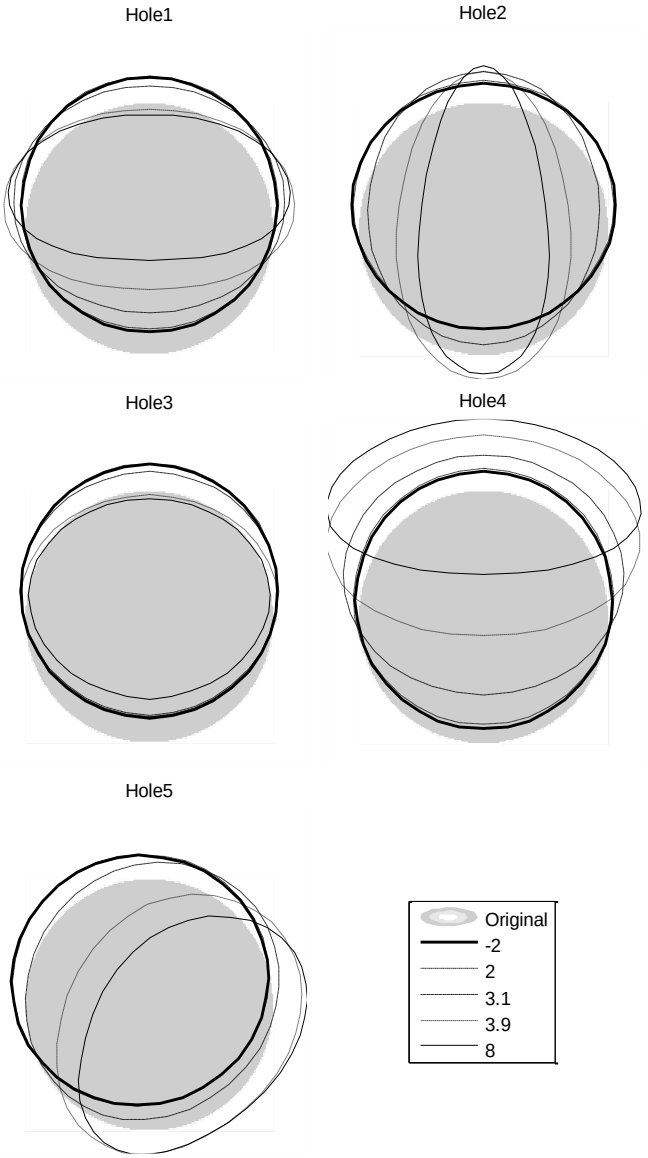

Fig 4. Hole deformation and drift for the five holes for different values of the non-dimensional friction parameter, $\log(k \times m/\eta)$. The vertical coincides with the radial direction for each hole. The shaded circle corresponds to the size (1 mm diameter) and relative location of the pin.

VI. Discussion

The extrusion study by Trabelssi et al. [22] for a solid glass preform for viscosity greater than 10^7 Pa·s showed that modeling slip with friction at the wall of the die is of primary importance and must be accounted for. From the point of view of material behavior, while modeling viscoelasticity enhances the precision of the model, purely viscous material behavior was shown to be an accurate first assumption that reduces computational cost. This reduction was offset by the added geometric complexity of MOF extrusion. In addition to

adding a series of holes with diameters that are much smaller than the diameter of the channel, an axisymmetric model can no longer be used since the die is fitted with an insert that breaks the symmetry and adds the feed hole and pin compartments.

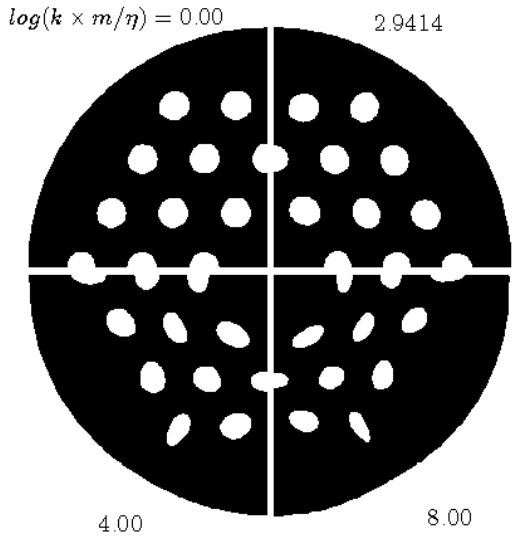

Fig 5. Preform geometry for different friction coefficients.

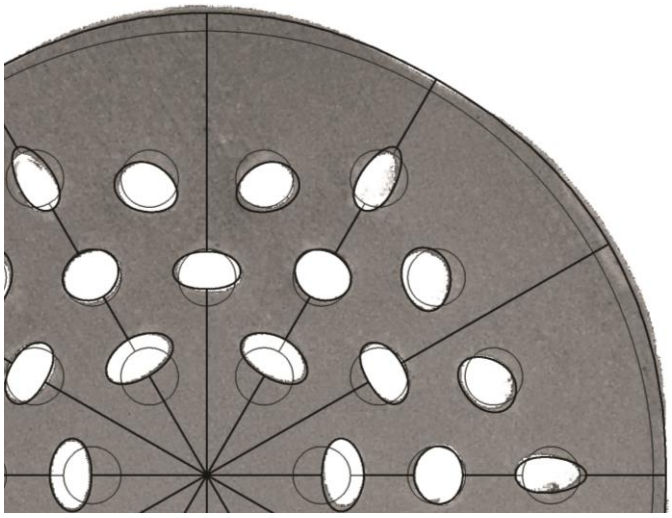

Fig 6. Visual validation of the hole shapes between a photograph of the actual preform [1] and the simulation for a normalized friction coefficient of 4.29. The original locations of the pins are also indicated.

The focus of the study was on how friction and die geometry lead to distortion and drift of the holes in the cross section. A specific geometry was addressed for which experimental data was used in a validation.

Friction is the most interesting quantity affecting the location and shape of each hole. As a general statement there are three ranges of friction: low friction where slight changes occur, high friction where an increase in friction does not have a significant effect and an "active" friction interval between the two where distortion is most sensitive to the level of friction. Within the active friction interval ($-1 < \log(k \times m/\eta) < 8$) there are complex competing mechanisms that lead to distortion. These mechanisms include die swell that is created upon exit from the die, which for such high viscosity and low ram speed extrusion tends to move material radially outward and is non-uniform in the circumferential direction.

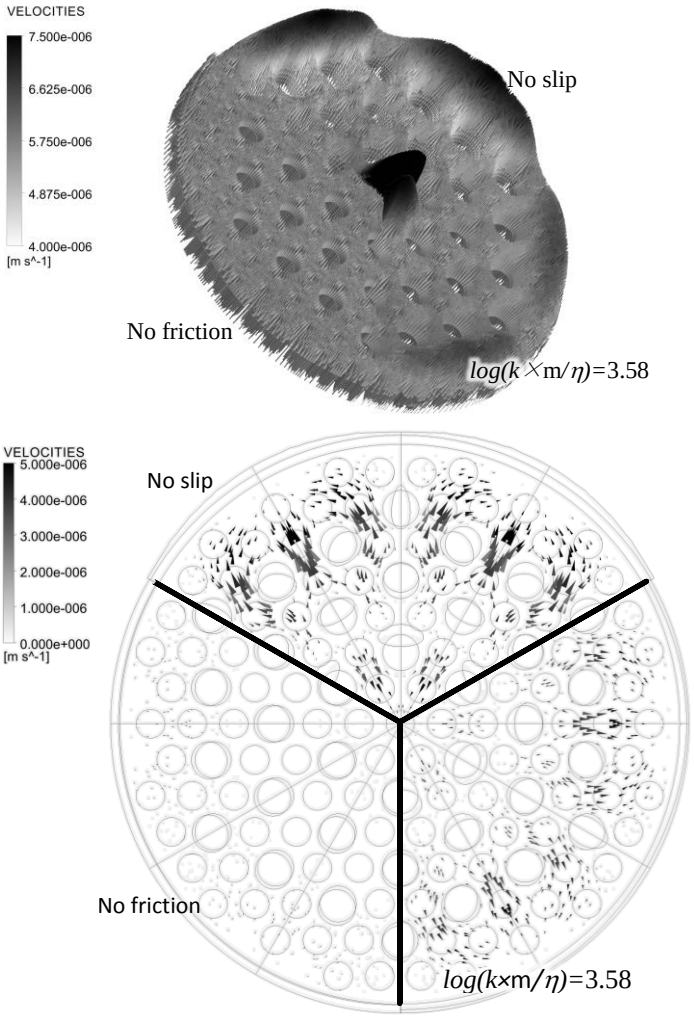

Fig 7. Flow profiles halfway through the welding chamber for no-slip, no friction and an intermediate value.

In addition in-plane flow and non-uniform axial flow occur within the welding chamber lead to hole distortion and drift as the flow exits from the tip of each of the pins. By far the most complex flow occurs within the welding chamber, the length of which is a very critical design parameter. If the welding chamber is too short, the proper merging of the flow might not occur. As the welding chamber length increases, the outcome becomes less affected by the feed hole distribution and eventually the flow will fully develop. In the high friction cases, however, even for a fully developed flow, non-uniform axial flow around the tip of a pin will contribute to distortion.

While the authors believe the experimental validation of the model implies that the assumptions are justified, ideally the friction coefficient would have been obtained in an independent test. The best available information for the normalized friction coefficient is the value of 3.55 that was obtained in [22] using F2 glass, as compared to the coefficient of 4.29 in the current study using SF57 glass for the same die material. Because of this limitation, questions can be raised on the relative importance of some factors that were neglected

in the modeling, such as gravitational effects, surface tension, temperature non-uniformity, and viscoelastic material behavior. The former two factors were neglected due to the high viscosity. The case of a viscoelastic material response was neglected due to the rather large computational burden it would add without the expectation of a significant change in results. Temperature non-uniformity within the die, especially in the radial direction, if significant, will change the results and as such, the applicability of the results in this study requires sufficient heating to reach a constant temperature. Experimentally, sufficient heating was employed by exposing glass and die to the target extrusion temperature for 30-40 min prior to applying a force and starting the flow through the extrusion die. Finally, depending on the method of die manufacture used, friction can vary between surfaces.

VII. Conclusion

Validation of the computational modeling approach for the extrusion of MOF preforms allows for the following conclusions:

- The complexity of distortion and drift of holes in a MOF can be predicted using an isothermal viscous model that accounts for interface slip with friction.
- Distortion tends to increase as friction increases and is present even for the case of no friction.
- The most complex flow occurs within the welding chamber and is most pronounced for high friction. For the cases considered in this study a fully developed flow profile was not reached within the welding chamber.
- The most affected holes are near the center and near the outer perimeter, consistent with experimental observations [1]. Furthermore, each hole deforms differently, which depends on position.

Acknowledgment

The authors thank Dr. B. Ananthasayanam for his help in providing the structural relaxation results.

VIII. References

[1] H. Ebendorff-Heidepriem and T.M. Monro, "Extrusion of complex preforms for microstructured optical fibers," Opt. Express, 15, 15086-15092 (2007).

[2] H. Ebendorff-Heidepriem, R.C. Moore and T.M. Monro, "Progress in the Fabrication of the Next-Generation Soft Glass Microstructured Optical Fibers," AIP Conference Proceedings, 1055, 95-98 (2008).

[3] J. C. Knight, "Photonic crystal fibres," Nature **424**, 847–851 (2003).

[4] P. St. J. Russell, "Photonic crystal fibers," Science **299**, 358–362 (2003).

[5] X. Feng, A.K. Mairaj, D.W. Hewak and T.M. Monro, "Nonsilica glasses for holey fibers," J. Lightwave Tech. **23**, 2046-2054 (2005).

[6] R. Kostecki, H. Ebendorff-Heidepriem, C. Davies, G. McAdam, S.C. Warren-Smith, T.M. Monro, "Silica exposed-core microstructured optical fibers," Optical Materials Express **2** (11), 1538-1547 (2012).

[7] M. El-Amraoui, G. Gadret, J. C. Jules, J. Fatome, C. Fortier, F. Désévédavy, I. Skripatchev, Y. Messaddeq, J. Troles, L. Brilland, W. Gao, T. Suzuki, Y. Ohishi, and F. Smektala, "Microstructured chalcogenide optical fibers from As_2S_3 glass towards new IR broadband sources," Opt. Express **18,** 26655–26665 (2010).

[8] Q. Coulombier, L. Brilland, P. Houizot, T. Chartier, T. N. N'Guyen, F. Smektala, G. Renversez, A. Monteville, D. Méchin, T. Pain, H. Orain, J. C. Sangleboeuf, and J. Trolès, "Casting method for producing low-loss chalcogenide microstructured optical fibers," Opt. Express, **18,** 9107–9112 (2010).

[9] A. Mori, "Tellurite-based fibers and their applications to optical communication networks," J. Ceram. Soc. Jpn. **116**, 1040–1051 (2008).

[10] T.M. Monro and H. Ebendorff-Heidepriem, "Progress in Microstructured Optical Fibers," Annu. Rev. Mater. Res., 36, 467–495 (2006).

[11] J. Bei, T.M. Monro, A. Hemming, H. Ebendorff-Heidepriem, "Fabrication of extruded fluoroindate optical fibers", Optical Materials Express **3** (3), 318-328 (2013).

[12] A. S. Webb, F. Poletti, D. J. Richardson, and J. K. Sahu, "Suspended-core holey fiber for evanescent-field sensing sensing," Opt. Eng. **46**, 010503 (2007).

[13] P. McNamara, D. G. Lancaster, R. Bailey, A. Hemming, P. Henry, and R. H. Mai, "A large core microstructured fluoride glass optical fiber for mid-infrared single-mode transmission," J. Non-Cryst. Solids 355, 1461-1467 (2009).

[14] H. Ebendorff-Heidepriem, T.-C. Foo, R. C. Moore, W. Zhang, Y. Li, T. M. Monro, A. Hemming, and D. G. Lancaster, "Fluoride glass microstructured optical fiber with large mode area and mid-infrared transmission," Optics Letters 33, 2861-2863 (2008).

[15] M.-J. Li, J.A. West and K.W. Koch, "Modeling Effects of Structural Distortions on Air-Core Photonic Bandgap Fibers," J. Lightwave Technol., 25, 2463-2468 (2007).

[16] S.K. Varshney, K. Saitoh, M. Koshiba and P.J. Roberts, "Analysis of a realistic and idealized dispersion compensating photonic crystal fiber Raman amplifier," Optical Fiber Technology, 13, 174-179 (2007).

[17] E.N. Fokoua, D.J. Richardson and F. Poletti, "Impact of structural distortions on the performance of hollow-core photonic bandgap fibers," Optics Express, 10, 2735-2744 (2014).

[18] B. Ananthasayanam, P.F. Joseph, D. Joshi, S. Gaylord, L. Petit, V.Y. Blouin, K.C. Richardson, D.L. Cler, M. Stairiker, M. Tardiff, "Final shape of precision molded optics: Part I – Computational approach, material definitions and the effect of lens shape," Journal of Thermal Stresses, 35, 550-578 (2012).

[19] B. Ananthasayanam, D. Joshi, M. Stairiker, M, Tardiff, K.C. Richardson and P.F. Joseph, "High Temperature Friction Characterization for Viscoelastic Glass Contacting a Mold," *Journal of Non-Crystalline Solids*, 385, 100-110 (2014).

[20] M. Trabelssi and P.F. Joseph, "Ring compression test for high temperature glass using the generalized Navier law, to appear, Journal of the American Ceramic Society.

[21] W. Egel-Hess and E. Roeder, "Extrusion of glass melt – influence of wall friction," *Glasstech. Ber.*, 62, 279–284 (1989).

[22] M. Trabelssi, H. Ebendorff-Heidepriem, K.C. Richardson, T.M. Monro and P.F. Joseph, "Computational Modeling of Die Swell of Extruded Glass Preforms at High Viscosity," Journal of the American Ceramic Society, 97, 1572-1581 (2014).

[23] H. Ebendorff-Heidepriem and T.M. Monro, "Analysis of glass flow during extrusion of optical fiber preforms," Opt. Mater. Express, 2, 304-320 (2012).

[24] B. Ananthasayanam, P.F. Joseph, D. Joshi, S. Gaylord, L. Petit, V.Y. Blouin, K.C. Richardson, D.L. Cler, M. Stairiker and M. Tardiff, "Final shape of precision molded optics: Part II—Validation and sensitivity to material properties and process parameters," J. Therm. Stresses, 35, 614-636 (2012).

[25] Patent WO2007/041791 or US2009/0220785 A1 "Method and device for forming microstructured fibre."

[26] M. Trabelssi, "Numerical analysis of the extrusion of fiber optic and photonic crystal fiber preforms near the glass transition temperature," Ph.D. Dissertation, Clemson University, May 2014.